

Towards Non-Parametric Models for Confidence Aware Image Prediction from Low Data using Gaussian Processes

Nikhil U. Shinde^{1*}, Florian Richter¹, Michael C. Yip¹

¹ University of California San Diego
 {nshinde, frichter, yip}@ucsd.edu

Abstract

The ability to envision future states is crucial to informed decision making while interacting with dynamic environments. With cameras providing a prevalent and information rich sensing modality, the problem of predicting future states from image sequences has garnered a lot of attention. Current state of the art methods typically train large parametric models for their predictions. Though often able to predict with accuracy, these models rely on the availability of large training datasets to converge to useful solutions. In this paper we focus on the problem of predicting future images of an image sequence from very little training data. To approach this problem, we use non-parametric models to take a probabilistic approach to image prediction. We generate probability distributions over sequentially predicted images and propagate uncertainty through time to generate a confidence metric for our predictions. Gaussian Processes are used for their data efficiency and ability to readily incorporate new training data online. We showcase our method by successfully predicting future frames of a smooth fluid simulation environment.

1 Introduction

Predicting future states is key to enabling smart decision making. As humans, we utilize predictions to inform daily decisions. This ranges from navigating through dense crowds to playing a game of tennis. Perfectly predicting such diverse phenomena requires distinct complex models that rely on underlying state information. However, humans are often able to make such predictions using imperfect models informed solely from visual input. Furthermore, we are able to adapt to and interact with constantly changing, new environments, after only a few observations. In this paper we focus on the task of predicting future images in an image sequence given a limited number of initial frames for context and training.

There has been a lot of research on video prediction. These works focus on predicting future image frames from videos in scenarios where a large amount of data is readily available to

train predictive models. Most current research leverages this data to train complex parametric models, like neural networks (NN), for video prediction. The high parameter count of these models increases their representational power and thus predictive accuracy. This high parameter count also necessitates large training datasets and prevents these models from usefully converging for the low data problem we consider.

The low data constraints of our problem statement impose certain desired solution criteria. We desire our proposed solution to have high predictive accuracy for short term predictions that stay close to the model’s training distribution. Since our problem statement limits this training distribution, we recognize that our model will have reduced long term prediction fidelity. It is also desirable for our model to be confidence aware. This means our model should recognize and provide an interpretable metric on how far the model has deviated from its training distribution. This will enable us to better contextualize our model’s predictions and make decisions based on whether our model’s predictive accuracy is compromised. We also desire the flexibility to readily expand our model’s training distribution, or shift it to only include recent data as previous datapoints become irrelevant.

To satisfy the desired solution criteria, we take a probabilistic approach to non-parametric image prediction using Gaussian Processes (GPs). GPs use a joint gaussian assumption on the distribution of the training data points to extrapolate predictions. This enables high quality predictions near the training distribution which can be readily expanded to include new observations. In particular, we utilize Gaussian Process Regression, which outputs gaussian distributions, parameterized by a mean and variance. While the mean acts as a good representation for the prediction, the variance serves as an interpretable metric of the model’s confidence in its predictions.

Short sequences of images contain a large amount of semantic and dynamic information that can be used to understand unseen environments. In many videos, such as satellite weather patterns, fluid motion, etc. the motion is repetitive, both temporally across different frames, and spatially within the same frame. We take advantage of this repetitiveness to train a predictive model using only a few images.

2 Related Works

Solutions for image sequence prediction problems often heavily rely on large datasets. There are several avail-

*Contact Author

able video datasets such as the Kitti ([Geiger *et al.*, 2013]), Camvid ([Brostow *et al.*, 2008]) and Caltech Pedestrian Dataset ([Dollar *et al.*, 2009]) for prevalent problems like autonomous driving. Some video datasets, such as the robot pushing dataset ([Finn *et al.*, 2016]), provide video data influenced by external controls for tasks like robot manipulation. To solve the problem settings captured by the aforementioned datasets, researchers train large parametric neural networks.

Most state of the art methods in video prediction build off of a few baseline neural network architectures: convolutional, recurrent and generative models. Convolutional Neural Networks, that rely on learning 2D convolutional kernels, enabled a breakthrough in problems in the image domain ([O’Shea and Nash, 2015]). They have also been extended to problems in video through 3D convolutions ([Wang *et al.*, 2019], [Aigner and Korner, 2018]). Recurrent Neural Networks (RNNs) ([Rumelhart *et al.*, 1986]) and LSTMs ([Hochreiter and Schmidhuber, 1997]) presented more principled architectures to handle the time dependencies that come with sequences of images. They have been leveraged by works such as [Chen *et al.*, 2017], [Wichers *et al.*, 2018], and [Walker *et al.*, 2017]. Generative adversarial networks directly model the generative distribution of the predicted images ([Goodfellow *et al.*, 2014]). To handle uncertainty some researchers have turned to using Variational Autoencoders ([Kingma and Welling, 2014]) and ensemble networks ([Talebzadeh and Moridnejad, 2011]). Most approaches employ combinations of these architectures to achieve state of the art results. Methods like [Yu *et al.*, 2020] and [Byeon *et al.*, 2018] use these methods to directly predict the pixels in future images. We take inspiration from this direct prediction approach, along with generative and convolutional approaches and design our method to directly generate distributions on output pixels while iterating over the image in a kernel like fashion.

There is also a large body of work on predicting and simulating fluids. The motion of incompressible fluids is governed by the Navier Stokes equations, a set of partially differentiable equations (PDEs). Modern techniques such as [Raissi *et al.*, 2019], [Jiang *et al.*, 2020], [Greenfeld *et al.*, 2019] and [Li *et al.*, 2021] use neural networks to learn to solve complex PDEs directly from data.

All the methods discussed above focus on a prediction problem where large representative datasets are readily available. In this paper we focus on the case when the available training data is limited to only a few frames. In these low data scenarios, the above methods often fail to converge to useful solutions. We choose Gaussian Process Regression as the core predictive component of our method. Gaussian Processes have been used across various robotic and machine learning applications to estimate highly nonlinear functions with probabilistic confidence ([Rasmussen and Williams, 2005]). These non-parametric models have been regularly used to estimate functions online with very little data. ([Ko *et al.*, 2007]) use a GP-enhanced reinforcement learning model to learn the blimp dynamics online. This model improves the state predictions of the traditional ODE modelling approach while also giving a useful uncertainty estimate. SOLAR-GP builds upon such system identifica-

tion approaches and uses localized sparse GP models to learn robot dynamics online to improve teleoperation ([Wilcox and Yip, 2020]). PILCO improves the system identification approach further by learning a probabilistic dynamics model ([Deisenroth and Rasmussen, 2011]). They propagate prediction uncertainty through time to facilitate long term planning and improve policy search methods for reinforcement learning with very little data collection. GP’s predictive uncertainty measure has also been widely used by the safety community. Safe IML uses GPs to estimate an environment’s safety function online ([Turchetta *et al.*, 2019]). They leverage the uncertainty outputted by the GP to provide safety guarantees and inform intelligent and risk aware exploration that does not compromise the robot’s safety. In this work we use GPs to predict future images from image sequences.

3 Background: Gaussian Processes

The core predictive component of our method uses a Single Output GP Regression Model. A GP models a function f , using training data $(X, f(X))$. $X = [x_0, x_1, \dots, x_{n-1}] \in \mathbb{R}^{n \times D}$ are all the training inputs and $f(x) = [f(x_0), \dots, f(x_{n-1})] \in \mathbb{R}^{n \times 1}$ are the training outputs. Given test inputs $X' \in \mathbb{R}^{m \times D}$ we want to find outputs $f(X')$. Let $X_A \in \mathbb{R}^{(m+n) \times D}$ refer to all the train and test inputs and $f(X_A)$ be the corresponding outputs. A GP relies on the assumption that all the outputs are characterized by a multivariate gaussian distribution $f(X_A) \sim \mathcal{N}(\mu(X_A), \Sigma_{X_A X_A})$. We assume the mean $\mu(X_A) = 0$, and the covariance matrix is characterized by a kernel function $k(x, y)$ such that $\Sigma_{X_A, X_A}[u, v] = k(X_A[u], X_A[v])$. To solve for the distribution of the test outputs $p(f(X')) \sim \mathcal{N}(\mu(X'), \Sigma_{X' X'})$ we use the marginal likelihood of a multivariate gaussian $p(f(X'|X, f(X), X'))$ to get:

$$\mu(X') = k(X', X)[k(X, X) + \sigma_n^2 I]^{-1} f(X) \quad (1)$$

$$\Sigma_{X' X'} = k(X', X') - k(X', X)[k(X, X) + \sigma_n^2 I]^{-1} k(X, X') \quad (2)$$

$k(X, X)[u, v] = k(X[u], X[v])$, $k(X, X) \in \mathbb{R}^{n \times n}$, $k(X', X)[u, v] = k(X'[u], X[v])$, $k(X', X) = k(X, X')^T \in \mathbb{R}^{m \times n}$, σ_n^2 is the noise variance, $I \in \mathbb{R}^{n \times n}$ is the identity matrix. To train the GP Regression model we optimize the noise variance, σ_n , and kernel parameters to maximize the log likelihood of the training data.

We use the Radial Basis Function (RBF) kernel:

$$k(x, y) = \alpha^2 \exp\left(-\frac{(x - y)^T \Lambda^{-1} (x - y)}{2}\right) \quad (3)$$

Kernel parameters, α and Λ , are optimized during training. For outputs of dimension $O > 1$, we train a GP for each dimension $a \in [0, O - 1]$. Each model has its own kernel $k_a(\cdot, \cdot)$, trained by optimizing its parameters $\sigma_{n,a}$, α_a and Λ_a .

4 Methods

4.1 Problem Statement and Prediction Framework

We define an image sequence as a sequence of frames $[z_0, z_1 \dots z_{t_0-1}, z_{t_0}, \dots z_{t-1}, z_t \dots]$. Here $z_i \in \mathbb{R}^{Q \times Q}$ denotes the i -th frame in the sequence. Given initial training frames $[z_0, \dots z_{t_0-1}]$, our objective is to predict frames

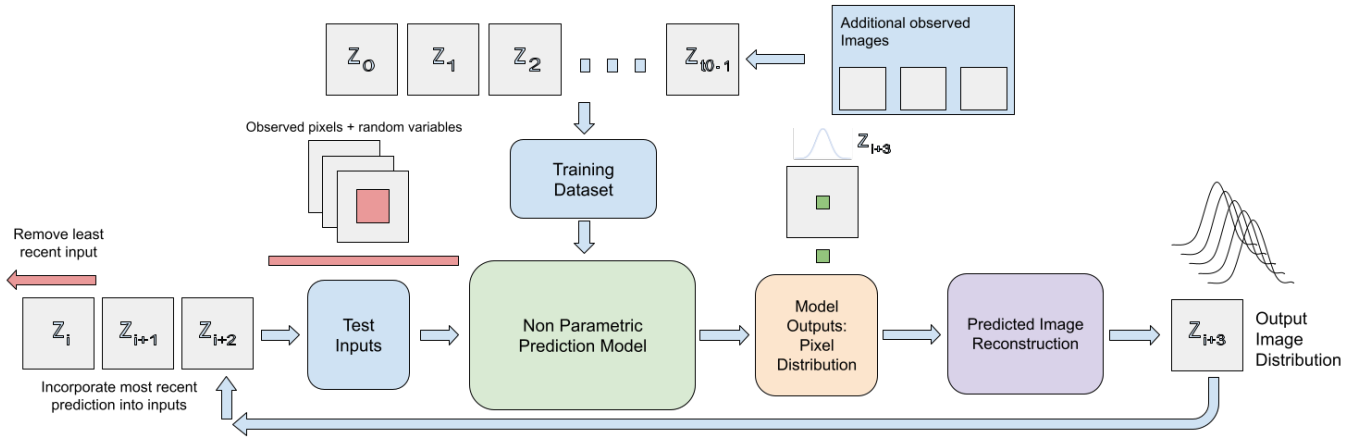


Figure 1: This figure shows an overview of the method. We begin by pre-processing the initial video frames $[z_0, \dots, z_{t_0-1}]$ to form the dataset to train a GP Regression model. During test time three sequential input images are processed into test inputs. Our trained model predicts output distributions from these test inputs. These distributions are then combined to form a predictive distribution of the image at the next time step. This predicted distribution image is then incorporated into the next set of input images and the rollout process is continued.

$[z_{t_0}, \dots, z_t, \dots]$. As additional frames $[z_{t_0}, \dots, z_{t'}]$ become available, they may be incorporated into the model’s training data to improve the accuracy of the future prediction.

We train a model to use recurring motion patterns to understand scene dynamics to predict future images. Our model learns and predicts on square image patches of dimension (p, p) . Predicting at this smaller scale enables us to better utilize our limited training data and extract smaller repeating patterns that are more likely to recur across space and time. Our method predicts one frame at a time given the 3 most recent, seen and predicted frames. We use 3 input frames to capture second order dynamics. We first convert input images into patches and then suitable inputs for our GP Regression models. The models output distributions on pixels in future images. These are combined to form a random variable image. The predicted image is incorporated into the next set of inputs and the process is repeated. Our method must handle a combination of random and known inputs, while propagating probability distributions through time.

4.2 Training

To construct our model, we begin by creating a training data set from frames $[z_0, \dots, z_{t_0-1}]$. We divide the images into sets of 4 sequential images $[z_i, z_{i+1}, z_{i+2}, z_{i+3}]$, $i \in [0, t_0 - 4]$. To create a datapoint we take p dimensional patches corresponding to the same pixel locations from each image. $z_i[k : k + p, l : l + p] \in \mathbb{R}^{p \times p}$ denotes a p by p patch in image z_i starting at pixel (k, l) . A training input, $x_j \in \mathbb{R}^{3p^2}$, is created by flattening and concatenating the patches from the first 3 images. The corresponding training output, $f(x_j) \in \mathbb{R}^{(p-b)^2}$, is created by flattening the corresponding patch from the 4th image z_{i+3} , cropped with a patch boundary term b : $z_{i+3}[k + b : k + p - b, l + b : l + p - b] \in \mathbb{R}^{(p-b) \times (p-b)}$. When $b > 0$, we do not predict the outer edges of the patch, where predictions may suffer due to contributions from the scene outside our input. Within each set of 4 sequential images, we sample data points with a stride of s pixels. In this

paper, we utilize a ‘wrapping’ approach to handle patches that extend beyond the edge of an image. This approach assumes the frame, z_i with g rows and f columns, captures a periodic environment where $z[g + i, f + j] = z[i - 1, j - 1]$ and $z[-i, -j] = z[g - (i + 1), f - (j + 1)]$. Approaches like padding frames or skipping incomplete patches are possible but not further explored in this paper. We repeat this sampling procedure for every set of images to create the training dataset with n data points: $(X, f(X)) = (x_j, f(x_j))$, $j \in [0, n - 1]$. $X \in \mathbb{R}^{n \times 3p^2}$ and $f(X) \in \mathbb{R}^{n \times (p-b)^2}$. This process is shown graphically in Figure 5 in section A.4

We create a GP Regression model for every output dimension $O = (p - b)^2$. Each model is trained by optimizing its noise, $\sigma_{n,a}$, and kernel parameters, α_a and Λ_a in $k_a(\cdot, \cdot)$, to maximize the log likelihood of the training data for output dimension $a \in [0, (p - b)^2 - 1]$. To predict future images, each GP model outputs a mean and variance corresponding to a pixel in the output patch. The predicted image z_i , is represented by a mean and variance image pair (M_i, V_i) . Each pixel in M_i and V_i corresponds to the mean and variance of the predicted random gaussian variable for that pixel location, respectively. Every future image pixel is predicted once.

4.3 Prediction

Once trained, we can use our model to rollout predictions for any T time steps into the future, starting from 3 known, consecutive input images $[z_i, z_{i+1}, z_{i+3}]$. We use a recursive method to predict multiple frames into the future. Our model takes the 3 most recently seen and predicted frames and uses them to predict one future frame, represented as a random variable. We incorporate this predicted random variable as the latest image in the 3 frame inputs to predict the next time step. This process is repeated to predict the desired T steps into the future. We start discussing our predictions in the context of predicting the fourth time step and onwards. Starting at the fourth prediction all the utilized input images are random variables previously outputted by our model. The first

three predictions incorporate known, observed input images and predicted random input images. These initializing predictions will be discussed as a special case of the more general prediction from all random variable input images.

We discuss the general method of predicting z_{i+3} from input images $[z_i, z_{i+1}, z_{i+2}]$, that are all random variables outputted by our model. To predict z_{i+3} , we first create a set of m test inputs $x'_j, j \in [0, m - 1]$. Each test input is a multivariate gaussian random variable composed of $3p^2$ independent gaussian random variables sampled from the input images. Since the input images are predicted random variables, our test inputs are created by sampling their corresponding mean and variance images: $[(M_i, V_i), (M_{i+1}, V_{i+1}), (M_{i+2}, V_{i+2})]$. We make simplifying assumptions that the predictions of each GP model as well as the outputs of the same model on different inputs are independent. Without assuming independence, we would have the computationally intractable task of tracking the covariance across all pixels. As a result of this assumption, the predicted images and their sub-patches can be flattened, concatenated and represented as one multivariate gaussian random variable. We use the patch based sampling method described in section 4.2, separately, on the sets of consecutive mean and variance images to generate the mean and variance test input vectors, $x'_{j,\mu} \in \mathbb{R}^{3p^2}$ and $x'_{j,\sigma} \in \mathbb{R}^{3p^2}$ respectively. These vectors specify the multivariate gaussian distribution of the input $x'_j \sim \mathcal{N}(x'_{j,\mu}, \Sigma_{x'_{j,\sigma}})$. To construct $\Sigma_{x'_{j,\sigma}}$, we use our independence assumptions such that the input covariance is a diagonal matrix with the vector of variances, $x'_{j,\sigma}$, along the diagonal. We adjust our sampling stride to generate an input to predict every pixel in the future image.

We discuss our method in the context of predicting a single output dimension $a \in [0, (p - b)^2 - 1]$ from a single input x'_j . Our model output is the predicted random variable $f(x'_j)[a]$. As in standard GP Regression, we are solving for the distribution of $p(f(x'_j)[a])$. We solve for $p(f(x'_j)[a])$ by marginalizing $p(f(x'_j)[a]|X, f(X), x'_j)$ over the input images.

$$p(f(x'_j)[a]) = \int_{-\infty}^{\infty} p(f(x'_j)[a]|x'_j, X, f(X)[:, a])p(x'_j)dx'_j \quad (4)$$

Solving this integral is analytically intractable. We approximate the posterior distribution from equation 4 to be Gaussian. Having the outputs form a multivariate gaussian, like the inputs, enables the predictions to be recursive. To solve for $p(f(x'_j)[a])$ we take advantage of this assumption and use moment matching in a method akin to [Deisenroth and Rasmussen, 2011]. Our method is distinguished from [Deisenroth and Rasmussen, 2011] in its use of multiple past states as inputs, prediction on images, and incorporation of known input states. Moment matching enables us to directly solve for the mean $\mu(x'_j)[a]$ and variance $\Sigma(x'_j)[a, a]$ of the outputted Gaussian distribution. This gives us the following formula to

predict the mean of an output pixel from all random inputs:

$$\begin{aligned} \mu(x'_j)[a] &= d_a^T \beta_a \\ d_a[i] &= \alpha_a^2 \cdot (|\Sigma_{x'_{j,\sigma}} \Lambda_a^{-1} + I|)^{-\frac{1}{2}} \cdot e^{-\frac{1}{2} v_i^T (\Sigma_{x'_{j,\sigma}} + \Lambda_a)^{-1} v_i} \quad (5) \\ \beta_a &= [k_a(X, X) + \sigma_n^2 I]^{-1} f(X)[:, a] \end{aligned}$$

Here $d_a \in R$ To predict variance from random inputs we use:

$$\begin{aligned} \Sigma(x'_j)[a, a] &= \alpha_a^2 - \text{trace}((k_a(X, X) + \sigma_n^2 I)^{-1} Q_{aa}) + \\ &\quad \beta_a^T Q_{aa} \beta_a - \mu(x'_j)[a] \quad (6) \\ Q_{aa}[i, k] &= k_a(x_i, x'_j) k_a(x_k, x'_j) \cdot |R|^{-\frac{1}{2}} \cdot e^{\frac{1}{2} z_{ik}^T R^{-1} \Sigma_{x'_{j,\sigma}} z_{ik}} \quad (7) \end{aligned}$$

Here $Q_{aa} \in \mathbb{R}^{n \times n}$, $R = \Sigma_{x'_{j,\sigma}} 2\Lambda_a^{-1} + I \in \mathbb{R}^{n \times n}$ and $z_{ik} = \Lambda_a^{-1} v_i + \Lambda_a^{-1} v_k$. A derivation of these equations, using moment matching, is discussed in the appendix A.2. These equations are used on all the test inputs to predict the mean and variance for every pixel in z_{i+3} . The predicted image z_{i+3} is stored as a mean, variance image tuple: (M_{i+3}, V_{i+3}) . To continue the predictive rollout we incorporate the latest prediction into a new set of input images $[z_{i+1}, z_{i+2}, z_{i+3}]$ to predict z_{i+4} . The mean images $[M_i, \dots, M_{i+3}, \dots]$ act as our predictions, while the variance images $[V_i, \dots, V_{i+3}, \dots]$ act as a confidence measure on our prediction.

In the first three predictions some or all of the input images are known, observed images. These predictions are initializing steps to begin the predictive rollout. The initializing predictions are special cases of the general prediction formulation with all random variable inputs. In this case we still treat all components of our input as random variables. We no longer treat the whole input as a single multivariate gaussian. We use our independence assumptions to disentangle the predictive method into parts that solely interact with the input dimensions contributed from the observed images, and those contributed from the predicted random variable images. We treat the random variable component of the input as a multivariate gaussian and use a delta function at the observed values as the joint probability distribution for the known component. We use these representations to re-derive the moment matching formulas. We walk through this method and provide formulas to predict the future pixel mean and variance in section A.1 of the Appendix. Figure 1 is an overview of the whole method.

5 Experiments and Results

We test our methods by predicting the vorticity of an incompressible fluid on a unit torus environment. Our data is computed using 2D Navier Stokes Equations. We generate our data with traditional PDE solvers using the code and approach detailed in [Li *et al.*, 2021]. The fluid simulation generates image sequences whose pixels change smoothly over both space and time. This environment is well suited to the RBF kernel. The dynamics of the toroidal environment wrap around the square image frame. This enables us to utilize the ‘‘Wrapping’’ approach when creating edge patches. Each image pixel is a float centered at 0. As a result, we directly predict future pixels using our 0 mean gp regression model. For

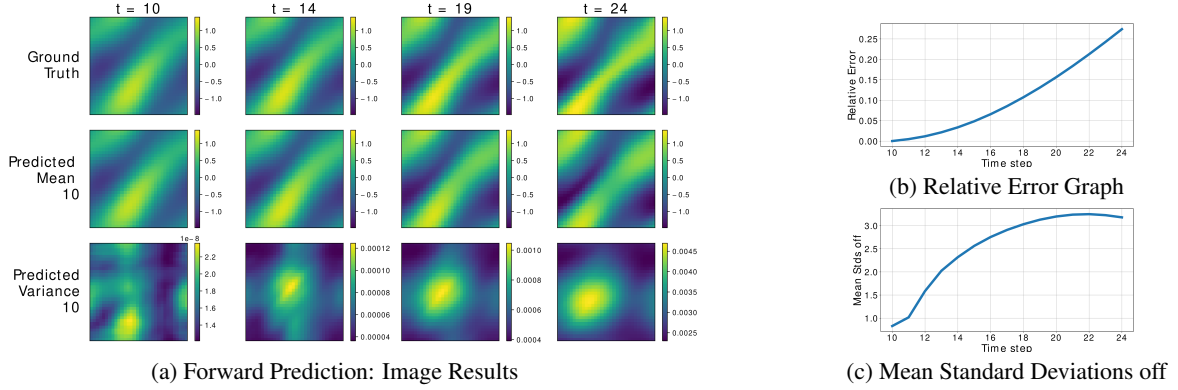


Figure 2: Forward Prediction Experiment: Our model, trained using frames $[z_0, \dots, z_9]$, is used to predict frames $[z_{10}, \dots, z_{24}]$ of a 2D Navier Stokes simulation. Figure (2a) shows the ground truth, predicted mean and variance images. Figure (2b) and Figure (2c) show graphs of the prediction’s relative error and mean standard deviations off. This shows our model’s ability to accurately predict dynamic scenes.

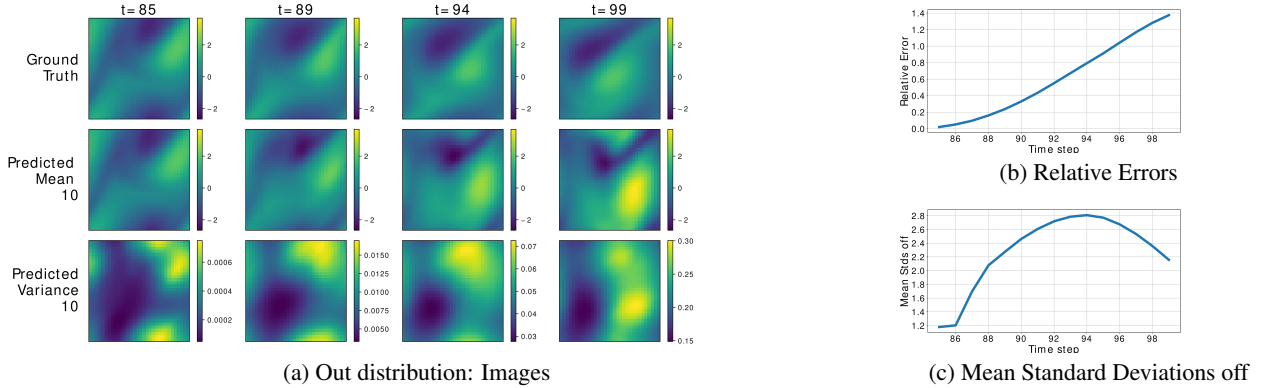


Figure 3: Out of distribution variance experiment: Our model is trained with frames $[z_0, \dots, z_9]$ of a 2d Navier Stokes simulation. We predict 15 frames from input images $[z_{82}, z_{83}, z_{84}]$, which generate inputs far from the model’s training distribution. The increase in the magnitude of the predicted variance, compared to the ‘In distribution’ predictions in Figure 2a, and low mean standard deviations off (Figure 3c) demonstrates our model’s understanding of its failure modes.

other data, we can predict on sequences of image differences which have the desired 0 mean property.

Each image, $z_t \in \mathbb{R}^{Q \times Q}$, in the image sequence represents the vorticity of the fluid at time t . We fix our fluid viscosity at $1e-3$, time step at $1e-4$ seconds and image resolution at $Q = 32$. Our experiments use input patch dimension $p = 15$ with patch boundary $b = 7$, resulting in $(1, 1)$ output patches. We utilize a single GP Regression model to predict this single output dimension. We generate training inputs using a stride of $s = 2$ and test inputs using test stride of $s = 1$. Each experiment predicts 15 frames into the future. The training images and initial input images are specified for each experiment.

We use two metrics: Relative error [Li *et al.*, 2021] ($RE(z, \tilde{z})$) and Mean Standard Deviations off ($StdE(z, \tilde{z}_\mu, \tilde{z}_\sigma)$) to analyze the performance of our model.

$$RE(z, \tilde{z}) = \|z - \tilde{z}\|_2 \cdot \|z\|_2^{-1} \quad (8)$$

$x \in \mathbb{R}^{Q \times Q}$ is the ground truth image, $\tilde{x} \in \mathbb{R}^{Q \times Q}$ is the predicted image and $\|\cdot\|_2$ is the 2 norm. This normalizes the

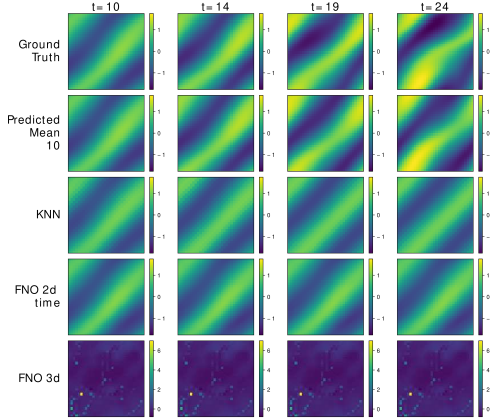
error with the magnitude of the original image

$$StdE(z, \tilde{z}_\mu, \tilde{z}_\sigma) = \frac{1}{Q^2} \sum_{i=0}^{Q-1} \sum_{j=0}^{Q-1} \left(\frac{|z[i, j] - \tilde{z}_\mu[i, j]|}{\sqrt{\tilde{z}_\sigma[i, j]}} \right) \quad (9)$$

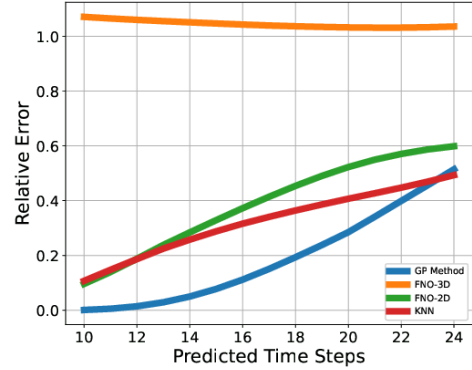
$z \in \mathbb{R}^{Q \times Q}$ is the ground truth image, $\tilde{z}_\mu, \tilde{z}_\sigma \in \mathbb{R}^{Q \times Q}$ is the predicted mean and variance images outputted by our model, and $|\cdot|$ is the absolute value function. This metric returns the average absolute standard deviations between our predicted mean image and the ground truth.

Forward Prediction Experiment: We train our model using the first $t_0 = 10$ frames of a video $[z_0, \dots, z_9]$. This model is used to predict the next 15 frames $[z_{10}, \dots, z_{24}]$, from input images $[z_7, z_8, z_9]$. The results of this experiment are shown in Figure 2. Our model’s predicted mean images track the complex dynamics of the ground truth with very little training data. The low magnitude of the variance images in Figure 2a indicates our model’s confidence in its predictions. This confidence is well founded given the low relative error in Figure 2b and low $StdE$ in Figure 2c which illustrate our ability to predict distributions that capture the ground truth.

Variance Experiments: The variance outputted by our



(a) Predictive Comparison Images



(b) Predictive Comparison Errors

Figure 4: Predictive Comparison Experiment: This figure compares the predictions on 2D Navier Stokes simulations between our method, a non-parametric KNN based method and the neural network based methods, FNO-2d-time and FNO-3d trained on similarly low data. Details are discussed in section. Figure 4 shows snapshots from predictions on a single test sequence. Figure 4b shows a graph of the relative error vs the predictive time step averaged across 100 prediction tests.

model acts as a confidence measure around the value of the corresponding predicted pixel mean. This variance is based on a kernel based metric evaluating the similarity between the model’s training data and the test input. To understand the variance output we look at a predictive rollout started with inputs far from our model’s training distribution. We use the same model trained in the ‘Forward Prediction’ experiment to predict frames $[z_{85}, \dots, z_{99}]$ from input images $[z_{82}, z_{83}, z_{84}]$. Since our environment changes slowly and smoothly over time, a large temporal gap increases the kernel based distance between the training and test data. The model recognizes that its inputs are too far from its training distribution to make a confident prediction. In response to the decrease in its predictive accuracy, the model increases its variance to track the increase in error keeping the *Std* low. The increase in variance magnitudes is very noticeable when contrasted with the variances in Figure 2a, where the inputs start close to the training distribution. The initial jump in the mean standard deviations off graphs indicates an initial overconfidence that the model quickly corrects. The results demonstrate our model’s ability to understand its failure modes with an interpretable confidence metric.

Predictive Comparison Experiment: We compare our method’s performance to the FNO2D-time and FNO 3D neural network methods in [Li *et al.*, 2021]. All methods are trained using similarly low number of training images. This experiment is solely a visual comparison, as such networks are not designs to be trained with such little data. We also contrast with a non-parametric K Nearest Neighbors approach. We set $k = 20$, use the same input and output preprocessing and utilize the same optimized RBF kernel based similarity metric to provide a fair comparison. The results in Figure 4 show our method outperforming the compared baselines. Both the neural networks and the KNN fail to learn the complex dynamics from the few available training frames, and simply output noise or sequences of identical frames. We

also show a graph of the relative error averaged over prediction experiments on 100 different Navier Stokes simulations.

Additional experiments and details on these experiments are presented in the supplementary material.

6 Conclusion and Future Discussion

In this paper we provided a novel method using non-parametric, GP-Regression models to predict probability distributions over future images in an image sequence with little training data. We showcased our method by predicting future image frames in a 2D Navier Stokes simulation environment. These experiments demonstrated our method’s ability to confidently capture the ground truth image sequence in our predicted image distribution for complex dynamic environments.

The problem statement of predicting future images from low data extends beyond the toy simulation environment presented in this paper. It is particularly applicable to tasks where collecting large representative datasets may be difficult or even unfeasible. Difficulties in data collection may stem from cost or regulatory restrictions. For tasks involving exploring novel unknown environments or where we are likely to encounter unexpected environmental variations, data collection may be outright unfeasible. Example use cases can be tasks in surgical and deep underwater environments or predictions on large scale unseen satellite weather patterns.

We seek to extend our methods to enable low data prediction of image sequences in the aforementioned scenarios. We wish to augment our predictive methods with the use of parametric deep learning techniques. Combining these methods can leverage out of distribution, but possibly pertinent, large datasets, while also taking into account small training datasets acquired locally and online. One prospective way to integrate the two methods is performing the prediction on top of deep features that we extract from real images. To further improve our method we also seek to extend our work to other kernel functions and remove some of our simplifying assumptions.

References

- [Aigner and Korner, 2018] Sandra Aigner and Marco Korner. Futuregan: Anticipating the future frames of video sequences using spatio-temporal 3d convolutions in progressively growing gans. *arXiv: Computer Vision and Pattern Recognition*, 2018.
- [Brostow *et al.*, 2008] Gabriel J. Brostow, Jamie Shotton, Julien Fauqueur, and Roberto Cipolla. Segmentation and recognition using structure from motion point clouds. In David Forsyth, Philip Torr, and Andrew Zisserman, editors, *Computer Vision – ECCV 2008*, pages 44–57, Berlin, Heidelberg, 2008. Springer Berlin Heidelberg.
- [Byeon *et al.*, 2018] Wonmin Byeon, Qin Wang, Rupesh Kumar Srivastava, and Petros Koumoutsakos. Contextvp: Fully context-aware video prediction, 2018.
- [Chen *et al.*, 2017] Xiongtao Chen, Wenmin Wang, Jinzhao Wang, and Weimian Li. Learning object-centric transformation for video prediction. In *Proceedings of the 25th ACM International Conference on Multimedia*, MM ’17, page 1503–1512, New York, NY, USA, 2017. Association for Computing Machinery.
- [Deisenroth and Rasmussen, 2011] Marc Peter Deisenroth and Carl Edward Rasmussen. Pilco: A model-based and data-efficient approach to policy search. In *Proceedings of the 28th International Conference on International Conference on Machine Learning*, ICML’11, page 465–472, Madison, WI, USA, 2011. Omnipress.
- [Dollar *et al.*, 2009] Piotr Dollar, Christian Wojek, Bernt Schiele, and Pietro Perona. Pedestrian detection: A benchmark. In *2009 IEEE Conference on Computer Vision and Pattern Recognition*, pages 304–311, 2009.
- [Finn *et al.*, 2016] Chelsea Finn, Ian Goodfellow, and Sergey Levine. Unsupervised learning for physical interaction through video prediction, 2016.
- [Geiger *et al.*, 2013] Andreas Geiger, Philip Lenz, Christoph Stiller, and Raquel Urtasun. Vision meets robotics: The kitti dataset. *International Journal of Robotics Research (IJRR)*, 2013.
- [Goodfellow *et al.*, 2014] Ian J. Goodfellow, Jean Pouget-Abadie, Mehdi Mirza, Bing Xu, David Warde-Farley, Sherjil Ozair, Aaron Courville, and Yoshua Bengio. Generative adversarial networks, 2014.
- [Greenfeld *et al.*, 2019] Daniel Greenfeld, Meirav Galun, Ron Kimmel, Irad Yavneh, and Ronen Basri. Learning to optimize multigrid pde solvers, 2019.
- [Hochreiter and Schmidhuber, 1997] Sepp Hochreiter and Jürgen Schmidhuber. Long short-term memory. *Neural Computation*, 9(8):1735–1780, 1997.
- [Jiang *et al.*, 2020] Chiyu Max Jiang, Soheil Esmailzadeh, Kamyar Azizzadenesheli, Karthik Kashinath, Mustafa Mustafa, Hamdi A. Tchelepi, Philip Marcus, Prabhat, and Anima Anandkumar. Meshfreeflownet: A physics-constrained deep continuous space-time super-resolution framework, 2020.
- [Kingma and Welling, 2014] Diederik P Kingma and Max Welling. Auto-encoding variational bayes, 2014.
- [Ko *et al.*, 2007] Jonathan Ko, Daniel J. Klein, Dieter Fox, and Dirk Haehnel. Gaussian processes and reinforcement learning for identification and control of an autonomous blimp. In *Proceedings 2007 IEEE International Conference on Robotics and Automation*, pages 742–747, 2007.
- [Li *et al.*, 2021] Zongyi Li, Nikola Kovachki, Kamyar Azizzadenesheli, Burigede Liu, Kaushik Bhattacharya, Andrew Stuart, and Anima Anandkumar. Fourier neural operator for parametric partial differential equations, 2021.
- [O’Shea and Nash, 2015] Keiron O’Shea and Ryan Nash. An introduction to convolutional neural networks, 2015.
- [Raissi *et al.*, 2019] M. Raissi, P. Perdikaris, and G.E. Karniadakis. Physics-informed neural networks: A deep learning framework for solving forward and inverse problems involving nonlinear partial differential equations. *Journal of Computational Physics*, 378:686–707, 2019.
- [Rasmussen and Williams, 2005] Carl Edward Rasmussen and Christopher K. I. Williams. *Gaussian Processes for Machine Learning (Adaptive Computation and Machine Learning)*. The MIT Press, 2005.
- [Rumelhart *et al.*, 1986] D. Rumelhart, Geoffrey E. Hinton, and Ronald J. Williams. Learning representations by back-propagating errors. *Nature*, 323:533–536, 1986.
- [Talebizadeh and Moridnejad, 2011] Mansour Talebizadeh and Ali Moridnejad. Uncertainty analysis for the forecast of lake level fluctuations using ensembles of ann and anfis models. *Expert Systems with Applications*, 38(4):4126–4135, 2011.
- [Turchetta *et al.*, 2019] Matteo Turchetta, Felix Berkenkamp, and Andreas Krause. Safe exploration for interactive machine learning, 2019.
- [Vinga, 2004] Susana Vinga. Convolution integrals of normal distribution functions. 01 2004.
- [Walker *et al.*, 2017] Jacob Walker, Kenneth Marino, Abhinav Gupta, and Martial Hebert. The pose knows: Video forecasting by generating pose futures, 2017.
- [Wang *et al.*, 2019] Yunbo Wang, Lu Jiang, Ming-Hsuan Yang, Li-Jia Li, Mingsheng Long, and Li. Fei-Fei. Eidetic 3d lstm: A model for video prediction and beyond. In *ICLR*, 2019.
- [Wichers *et al.*, 2018] Nevan Wichers, Ruben Villegas, Dumitru Erhan, and Honglak Lee. Hierarchical long-term video prediction without supervision, 2018.
- [Wilcox and Yip, 2020] Brian Wilcox and Michael C. Yip. Solar-gp: Sparse online locally adaptive regression using gaussian processes for bayesian robot model learning and control. *IEEE Robotics and Automation Letters*, 5(2):2832–2839, 2020.
- [Yu *et al.*, 2020] Wei Yu, Yichao Lu, Steve Easterbrook, and Sanja Fidler. Efficient and information-preserving future frame prediction and beyond. In *International Conference on Learning Representations*, 2020.

A Appendix

A.1 Predictions: The first 3 Predictions in a sequence of predictions

The first three predictions of a rollout involve predicting from a combination of known and predicted random variable sets of input images. We treat these predictions as special cases of the more general case presented in Section 4.3. Each input x'_j is composed of $3p^2$ independent random variables, with p^2 random variables contributed from each input image. We separate the input x'_j along the dimensions of the input that are known and random, to handle the different components separately. $x'_{j,Rn}$ and $x'_{j,Kn}$ are random variables that denote the random and known components of the input respectively. X_{Rn} , X_{Kn} and $x_{i,Rn}$, $x_{i,Kn}$ reference the corresponding known and random dimensions in all the training inputs and a single training input respectively.

The kernel functions k_a and the probability distribution over the input $p(x'_j)$ are the only forms of interaction with the inputs while predicting the output distribution $p(f(x'_j)[a])$. The structure of these functions and our independence assumptions allow us to cleanly split up our inputs into known and random components. We use the Radial Basis Function (equation 3) as our kernel function $k_a(x, y)$. In this function the inputs interact with one another along the same dimension, allowing us to re-write the kernel as:

$$\begin{aligned} k_a(x, y) &= \alpha_a^2 \exp\left(-\frac{(x-y)^T \Lambda_a^{-1} (x-y)}{2}\right) = \alpha_{a,Kn}^2 \cdot \\ &\exp\left(-\frac{(x_{Kn} - y_{Kn})^T \Lambda_{a,Kn}^{-1} (x_{Kn} - y_{Kn})}{2}\right) \cdot \\ &\alpha_{a,Rn}^2 \exp\left(-\frac{(x_{Rn} - y_{Rn})^T \Lambda_{a,Rn}^{-1} (x_{Rn} - y_{Rn})}{2}\right) \\ &= k_{a,Kn}(x_{Kn}, y_{Kn}) \cdot k_{a,Rn}(x_{Rn}, y_{Rn}) \end{aligned} \quad (10)$$

The subscripts on the inputs correspond to their known and random dimensions. $k_{a,Rn}$ and $k_{a,Kn}$ are the kernel functions that act on the known and random dimensions respectively. Each are parameterized by their own set of kernel parameters: $\alpha_{a,Kn}$, $\Lambda_{a,Kn}$ and $\alpha_{a,Rn}$, $\Lambda_{a,Rn}$ respectively. $\alpha_{a,Rn} \cdot \alpha_{a,Kn} = \alpha_a$. $\Lambda_{a,Kn}$ and $\Lambda_{a,Rn}$ are block diagonal matrices sampled from Λ_a , a large diagonal matrix, along the known and random dimensions. Using our assumption that all predicted pixels within and across images are independent, we separate the probability distribution:

$$p(x'_j) = p(x'_{j,Kn}) \cdot p(x'_{j,Rn}) \quad (11)$$

$p(x'_{j,Rn})$ is a multivariate gaussian distribution of the random components of the input and $p(x'_{j,Kn})$ denotes the joint distribution of all the known input pixels.

We construct our inputs according to this split input structure. The random component of each input is a multivariate gaussian distribution, $x'_{j,Rn} \sim \mathcal{N}(x'_{j,\mu}, \Sigma_{x'_{j,\sigma}})$, specified by its mean and covariance matrix. To create $x'_{j,\mu}$ and $\Sigma_{x'_{j,\sigma}}$

for the random test inputs, we use the method described in Section 4.3. We sample and concatenate patches from the mean and variance images corresponding to the subset of input images that are random variables. Pixels in the analogous patches of the known input images are flattened and concatenated to form $x'_{j,Kn,\mu}$, the observed values of $x'_{j,Kn}$ the random variable that is the known component of the test input. If all the input images are known, the test inputs are created in the same manner as the training inputs, as described in section 4.2

Our model output is the predicted random variable $f(x'_j)[a]$. To solve for our model's output, we must find the distribution $p(f(x'_j)[a])$ by solving the intractable integral in equation 4. We approach a solution with the same moment matching procedure presented in section 4.3, using the split kernel (equation 10) and probability distribution (equation 11) derived above. The values of the known pixels have been definitively observed with the assumption of no noise. The joint probability distribution of all known pixels can be substituted with a delta function at the observed values: $\delta(x - x'_{j,Kn,\mu})$. This allows us to integrate out certain contributions from the known components during the moment matching steps. Solving for the mean of $f(x'_j)[a]$ using these hybrid inputs we get:

$$\begin{aligned} \mu(x'_j) &= d_{a,hybrid}^T \beta_a \\ d_{a,hybrid}[i] &= k_{a,Kn}(x_{i,Kn}, x'_{j,Kn,\mu}) \cdot \\ &\frac{\alpha_{a,Rn}^2}{\sqrt{|\Sigma_{x'_{j,\sigma}} \Lambda_{a,Rn}^{-1} + I|}} \cdot e^{-\frac{1}{2} v_{i,Rn}^T (\Sigma_{x'_{j,\sigma}} + \Lambda_{a,Rn})^{-1} v_{i,Rn}} \end{aligned} \quad (12)$$

We use the \cdot operator to denote element wise multiplication. β_a is defined in equation 5 and $v_{i,Rn} = x'_{j,\mu} - x_{i,Rn}$. Solving for the variance of $f(x'_j)[a]$ from the hybrid inputs we get:

$$\begin{aligned} \Sigma(x'_j)[a, a] &= \alpha_a^2 - \text{trace}((k_a(X, X) + \sigma_{n,a}^2 I)^{-1} Q_{aa,hybrid}) + \\ &\beta_a^T Q_{aa,hybrid} \beta_a - \mu(x'_j)[a] \\ Q_{aa,hybrid} &= Q_{aa,Kn} \cdot Q_{aa,Rn} \\ Q_{aa,Kn} &= k_{a,Kn}(x'_{j,Kn,\mu}, X_{Kn})^T \\ k_{a,Kn}(x'_{j,Kn,\mu}, X_{Kn}) &\in \mathbb{R}^{n \times n} \\ Q_{aa,Rn}[i, k] &= \frac{1}{\sqrt{|R_{Rn}|}} \cdot \\ &k_{a,Rn}(x_{i,Rn}, x'_{j,\mu}) k_{a,Rn}(x_{k,Rn}, x'_{j,\mu}) \cdot e^{\frac{1}{2} z_{ik,Rn}^T R_{Rn}^{-1} \Sigma_{x'_{j,\sigma}} z_{ik,Rn}} \end{aligned} \quad (13)$$

$R_{Rn} = \Sigma_{x'_{j,\sigma}} (2\Lambda_{a,Rn}^{-1}) + I$ and $z_{ik,Rn} = \Lambda_{a,Rn}^{-1} v_{i,Rn} + \Lambda_{a,Rn}^{-1} v_{k,Rn}$. We use these equations to predict every pixel in the future image. Specific details for each step of the rollout are discussed in section A.3 A walkthrough derivation of these equations along with the specifics for each step of the rollout can also be found in section A.3.

A.2 Prediction with all random inputs: Derivations

In this section we discuss the derivations for the equations 5 and 6. These equations predict the mean and variance of the output distribution of a single pixel in a future image $p(f(x'_j)[a])$. These predictions are done from input x'_j which is a multivariate gaussian random variable $x'_j \sim \mathcal{N}(x'_{j,\mu}, \Sigma_{x'_{j,\sigma}})$ defined in section 4.3.

Mean Prediction Derivation: We begin by walking through the derivation of the mean $\mu(x'_j)[a]$ of the output distribution $p(f(x'_j)[a])$ presented in equation 5. For the following derivations we simplify the notation from $p(f(x'_j)[a]|x'_j, X, f(X)[:, a])$ to $p(f(x'_j)[a]|x'_j)$ as X and $f(X)[:, a]$ are known quantities. We begin our moment matching based derivation by taking the mean of the intractable integral presented in equation 4.

$$\begin{aligned} \mu(x'_j)[a] &= E_f \left[\int_{-\infty}^{\infty} p(f(x'_j)[a]|x'_i) p(x'_j) dx'_i \right] \\ &= E_{f, x'_j} [p(f(x'_j)[a]|x'_j)] \\ &= E_{x'_j} [E_f [p(f(x'_j)[a]|x'_j)]] \end{aligned} \quad (14)$$

$E_f [p(f(x'_j)[a]|x'_j)]$ is the analytical form of the mean during Gaussian Process Regression from equation 1. Substituting this formula into the above equations we get:

$$\mu(x'_j)[a] = E_{x'_j} [k_a(x'_j, X) [k_a(X, X) + \sigma_{n,a}^2 I]^{-1} f(X)[:, a]] \quad (15)$$

We denote $\beta_a \in \mathbb{R}^n$ to be $[k_a(X, X) + \sigma_n^2 I]^{-1} f(X)[:, a]$. We denote $d_a \in \mathbb{R}^n$ to be $E_{x'_j} [k_a(x'_j, X)]$.

$$d_a[i] = \int_{-\infty}^{\infty} k_a(x'_j, x_i) p(x'_j) dx'_j \quad (16)$$

$$\mu(x'_j)[a] = d_a^T \beta_a = \beta_a^T d_a \in \mathbb{R} \quad (17)$$

Expanding k_a to the RBF kernel equations and $p(x'_j)$ to the multivariate gaussian pdf, we solve for d_a using [Vinga, 2004]. This gives us the mean prediction equations listed in 5 and relisted below in equation 18:

$$\begin{aligned} \mu(x'_j)[a] &= d_a^T \beta_a \\ d_a[i] &= \frac{\alpha_a^2}{\sqrt{|\Sigma_{x'_{j,\sigma}} \Lambda_a^{-1} + I|}} e^{-\frac{1}{2} v_i^T (\Sigma_{x'_{j,\sigma}} + \Lambda_a)^{-1} v_i} \\ \beta_a &= [k_a(X, X) + \sigma_n^2 I]^{-1} f(X)[:, a] \end{aligned} \quad (18)$$

Variance Prediction Derivation: We now walk through the derivation of the predicted variance $\Sigma(x'_i)[a, a] \in \mathbb{R}$. Let $\Sigma(x'_i) \in \mathbb{R}^{(p-b)^2 \times (p-b)^2}$ be the covariance matrix of the predicted output, where $\Sigma(x'_i)[a, a] \in \mathbb{R}$ is the variance of output $f(x'_i)[a]$. Due to our independence assumptions between

outputted pixel distributions, we assert that the covariance between outputs $f(x'_j)[a]$ and $f(x'_j)[b]$, representing different output dimensions, $\Sigma(x'_i)[a, b] = 0, \forall a \neq b$.

$$\Sigma(x'_j) = E_{x'_j} \left[\left(f(x'_j) - \mu(x'_j) \right)^T \left(f(x'_j) - \mu(x'_j) \right) \right] \quad (19)$$

This is simplified using the law of total variance.

$$\begin{aligned} \Sigma(x'_j)[a, a] &= E_{x'_j} \left[\text{var}_f(f(x'_j)[a]|x'_j) \right] + \\ &E_{f, x'_j} \left[f(x'_j)[a] f(x'_j)[a] \right] - \mu(x'_j)[a]^2 \end{aligned} \quad (20)$$

$$\begin{aligned} E_{f, x'_j} \left[f(x'_j)[a] f(x'_j)[a] \right] &= \\ \int_{-\infty}^{\infty} E_f \left[f(x'_j)[a]|x'_j \right] E_f \left[f(x'_j)[a]|x'_j \right] p(x'_j) dx'_j \end{aligned} \quad (21)$$

$E_f \left[f(x'_j)[a]|x'_j \right]$ is the mean output of standard Gaussian Process Regression from equation 1.

Substituting this into the above equations we have:

$$\begin{aligned} &E_{f, x'_j} \left[f(x'_j)[a] f(x'_j)[a] \right] \\ &= \int_{-\infty}^{\infty} \beta_a^T k_a(x'_j, X)^T k_a(x'_j, X) \beta_a p(x'_j) dx'_j \\ &= \beta_a^T \int_{-\infty}^{\infty} k_a(x'_j, X)^T k_a(x'_j, X) p(x'_j) dx'_j \beta_a \end{aligned} \quad (22)$$

We define $Q_{aa} = \int_{-\infty}^{\infty} k_a(x'_j, X)^T k_a(x'_j, X) p(x'_j) dx'_j \in \mathbb{R}^{(p-b)^2 \times (p-b)^2}$. β_a is defined in the above sections. This gives us:

$$\begin{aligned} E_{f, x'_i} \left[f(x'_i)[a] f(x'_i)[a] \right] &= \beta_a^T Q_{aa} \beta_a \\ Q_{aa}[i, k] &= \frac{k_a(x_i, x'_j) k_a(x_k, x'_j)}{\sqrt{|R|}} e^{z_{ik}^T \mathbb{R}^{-1} \Sigma_{x'_{j,\sigma}} z_{ik}} \end{aligned} \quad (23)$$

$z_{ik} = \Lambda_a^{-1} v_i + \Lambda_a^{-1} v_k$ and $R = \Sigma_{x'_{j,\sigma}} [\Lambda_a^{-1} + \Lambda_a^{-1}] + I$ where $I \in \mathbb{R}^{n \times n}$ is the identity matrix.

In the first term of equation 20, $E_{x'_j} \left[\text{var}_f(f(x'_j)[a]|x'_j) \right]$, $\text{var}_f(f(x'_j)[a]|x'_j)$ is the variance output of Gaussian Process Regression from equation 2. Simplifying this term we get:

$$\begin{aligned} E_{x'_j} \left[\text{var}_f(f(x'_j)[a]|x'_j) \right] &= \alpha^2 - \\ &\text{trace} \left((k_a(X, X) + \sigma_{n,a}^2 I)^{-1} Q_{aa} \right) \end{aligned} \quad (24)$$

We substitute the equations from 24, 23 and 5 into equation 20 to compute the variance for each outputted pixel corresponding to output dimensions $a \in [0, (p-b)^2 - 1]$. This results in the variance prediction formula presented in equations 6 and 7 and relisted below as equations 25 and 26

$$\begin{aligned} \Sigma(x'_j)[a, a] &= \alpha_a^2 - \text{trace} \left((k_a(X, X) + \right. \\ &\left. \sigma_{n,a}^2 I)^{-1} Q_{aa} \right) + \beta_a^T Q_{aa} \beta_a - \mu(x'_j)[a] \end{aligned} \quad (25)$$

$$Q_{aa}[i, k] = \frac{k_a(x_i, x'_j) k_a(x_k, x'_j)}{\sqrt{|R|}} e^{\frac{1}{2} z_{ik}^T \mathbb{R}^{-1} \Sigma_{x'_{j,\sigma}} z_{ik}} \quad (26)$$

A.3 Prediction with Hybrid and Fully Known inputs: Derivations and Additional Details

In this section we discuss the derivations for the equations 12 and 13. These equations predict the mean and variance of the output distribution of a single pixel in a future image $p(f(x'_j)[a])$. These predictions are done from input x'_j which is composed of two random variables $x'_{j,Rn}$ and $x'_{j,Kn}$ explained in section A.3.

Mean Prediction Derivation: In this section we discuss the derivation of the mean prediction $\mu(x'_j)[a]$ of the output distribution $p(f(x'_j)[a])$ when using a combination of known and random input images, for the first 3 predictions of a rollout. We show the derivation for equation 12. Since this is a special case of prediction from all random inputs we begin our derivation from the derivation of the mean prediction equations for all random inputs in section A.2 We begin our derivation from equations 15, 16 and 17.

In this derivation we use the split kernel and probability density functions in equations 10 and 11 to deal with the hybrid, random and known, nature of the inputs. The joint probability distribution of all known pixels can be substituted with a delta function at the known values: $\delta(x - x'_{j,Kn,\mu})$. This allows us to integrate out certain contributions from the known components. β_a , being a constant, remains unchanged and we re derive d_a as $d_{a,hybrid}$.

$$\begin{aligned} d_{a,hybrid}[i] &= E_{x'_j}[k_a(x'_j, X[i])] \\ &= E_{x'_{j,Rn}, x'_{j,Kn}} [k_{a,Rn}(x'_{j,Rn}, X_{Rn}[i])k_{a,Kn}(x'_{j,Kn}, X_{Kn}[i])] \\ &= E_{x'_{j,Rn}} [k_{a,Rn}(x'_{j,Rn}, X_{Rn})] E_{x'_{j,Kn}} [k_{a,Kn}(x'_{j,Kn}, X_{Kn})] \\ &= \int_{-\infty}^{\infty} k_{a,Kn}(x'_{j,Kn}, X_{Kn}) \delta(x'_{j,Kn,\mu} - x'_{j,Kn}) dx'_{j,Kn} \\ &\quad \int_{-\infty}^{\infty} k_{a,Rn}(x'_{j,Rn}, X_{Rn}) p(x'_{j,Rn}) dx'_{Rn} \end{aligned} \quad (27)$$

Solving this yields the mean prediction for the third rollout given in equation 12 relisted below as equation 28:

$$\begin{aligned} \mu(x'_j) &= d_{a,hybrid}^T \beta_a \\ d_{a,hybrid}[i] &= k_{a,Kn}(x_{i,Kn}, x'_{j,Kn,\mu}) \cdot \frac{\alpha_{a,Rn}^2}{\sqrt{|\Sigma_{x'_{j,\sigma}} \Lambda_{a,Rn}^{-1} + I|}} \\ &\quad e^{-\frac{1}{2} v_{i,Rn}^T (\Sigma_{x'_{j,\sigma}} + \Lambda_{a,Rn})^{-1} v_{i,Rn}} \end{aligned} \quad (28)$$

Variance Prediction Derivation: Here we discuss the derivation of the variance $\Sigma(x'_j)[a, a] \in R$ in equation 13 from hybrid and random inputs. We follow the method outlined in the derivation for all random inputs. We use the split kernel and probability density functions in equations 10 and 11 to separately deal with the random and known components of the inputs. With this we arrive at an identical formulation to the case with all random inputs where $Q_{aa,hybrid}$ is used

in place of Q_{aa} .

$$\begin{aligned} Q_{aa,hybrid} &= E_{x'_j} [k_a(x'_j, X)^T k_a(x'_j, X)] \\ &= E_{x'_{j,Rn}} [k_{a,Rn}(x'_{j,Rn}, X_{Rn})^T k_{a,Rn}(x'_{j,Rn}, X_{Rn})] \\ &\quad E_{x'_{j,Kn}} [k_{a,Kn}(x'_{j,Kn}, X_{Kn})^T k_{a,Kn}(x'_{j,Kn}, X_{Kn})] \\ &= \int_{-\infty}^{\infty} k_{a,Kn}(x'_{j,Kn}, X_{Kn})^T k_{a,Kn}(x'_{j,Kn}, X_{Kn}) \\ &\quad \delta(x'_{j,Kn} - x'_{j,Kn,\mu}) dx'_{j,Kn} \\ &\quad \int_{-\infty}^{\infty} k_{a,Rn}(x'_{j,Rn}, X_{Rn})^T k_{a,Rn}(x'_{j,Rn}, X_{Rn}) p(x'_{j,Rn}) dx'_{Rn} \end{aligned} \quad (29)$$

Here \cdot denotes the element wise multiplication operator. The integrals with the multivariate gaussian pdfs result in the same solution as elaborated in the random variance derivation. Solving this yields the variance prediction given in equation 13 relisted below as equation 30:

$$\begin{aligned} \Sigma(x'_j)[a, a] &= \alpha_a^2 - \\ &\quad trace((k_a(X, X) + \sigma_{n,a}^2 I)^{-1} Q_{aa,hybrid}) + \\ &\quad \beta_a^T Q_{aa,hybrid} \beta_a - \mu(x'_j)[a]^2 \\ Q_{aa,hybrid} &= Q_{aa,Kn} \cdot Q_{aa,Rn} \\ Q_{aa,Kn} &= k_{a,Kn}(x'_{j,Kn,\mu}, X_{Kn})^T k_{a,Kn}(x'_{j,Kn,\mu}, X_{Kn}) \in \mathbb{R}^{n \times n} \\ Q_{aa,Rn}[i, k] &= \frac{1}{\sqrt{|R_{Rn}|}} \cdot k_{a,Rn}(x_{i,Rn}, x'_{j,\mu}) k_{a,Rn}(x_{k,Rn}, x'_{j,\mu}) \\ &\quad e^{\frac{1}{2} z_{ik,Rn}^T R_{Rn}^{-1} \Sigma_{x'_{j,\sigma}} z_{ik,Rn}} \end{aligned} \quad (30)$$

Rollout Discussion: In this section we discuss the composition of our inputs and additional details of each step in our predictive rollout. In a predictive rollout we are predicting T time steps into future starting from 3 known, consecutive input images $[z_i, z_{i+1}, z_{i+2}]$. With each prediction we predict a single time step into the future before incorporating our prediction into our next set of inputs. We continue this process until we predict the desired number of time steps.

First Step: The first step of the predictive rollout predicts z_{i+3} from input images $[z_i, z_{i+1}, z_{i+2}]$. For this first prediction all the input images are known quantities. As a result for each test input $x'_j \in [0, m-1]$, the entire test input is known, $x'_j = x'_{j,Kn}$, and $x'_{j,Rn}$ does not exist. $x'_{j,Kn,\mu} \in \mathbb{R}^{3p^2}$ is formed in a manner identical to the training inputs. When plugging these inputs into the hybrid mean prediction equation 12 and variance prediction equation 13 we remove the random components of the equations giving us:

$$d_{a,hybrid}[i] = k_{a,Kn}(x_{i,Kn}, x'_{j,Kn,\mu}) \quad (31)$$

$$Q_{aa,hybrid} = Q_{aa,Kn} \quad (32)$$

Substituting these back into the equations 12 and 13 we get the formulas to predict a single output dimension of for a single test input for the first prediction. These equations equivalent to the basic Gaussian Process Regression equations for

mean and variance prediction. Using these formulas we predict the distribution for every pixel in z_{i+3} from the m test inputs. This gives us the final predicted image z_{i+3} which is stored as a mean, variance image tuple (M_{i+3}, V_{i+3}) .

Second Step: The second step of the predictive rollout predicts z_{i+4} from input images $[z_{i+1}, z_{i+2}, z_{i+3}]$. z_{i+3} is a random variable, from the first prediction, represented by the mean and variance image tuple (M_{i+3}, V_{i+3}) . z_{i+1} and z_{i+2} are known. When constructing each test input, $x'_{j,Kn,\mu}$ is constructed from flattened and concatenated patches of $[z_{i+1}, z_{i+2}]$. $x'_{j,\mu}$ is constructed from flattened patches of M_{i+3} and $x'_{j,\sigma}$ is constructed from flattened patches of V_{i+3} to create the random input $x'_{j,Rn}$. These components together form a single test input x'_j . We plug these inputs into the hybrid mean prediction equation 12 and variance prediction equation 13 to compute the model's output distribution for a single output dimension. We repeat this to predict the output distributions for each pixel in the future image z_{i+4} which is stored as a mean and variance image tuple (M_{i+4}, V_{i+4}) .

Third Step: The third step of the predictive rollout predicts z_{i+5} from input images $[z_{i+2}, z_{i+3}, z_{i+4}]$. z_{i+3} and z_{i+4} are random variables, from the first and second predictions, represented by the mean and variance image tuples $(M_{i+3}, V_{i+3}), (M_{i+4}, V_{i+4})$. z_{i+2} is known. When constructing each test input, $x'_{j,Kn,\mu}$ is constructed from flattened patches of $[z_{i+2}]$. $x'_{j,\mu}$ is constructed from flattened concatenated patches of M_{i+3}, M_{i+4} and $x'_{j,\sigma}$ is constructed from flattened patches of V_{i+3}, V_{i+4} to create the random input $x'_{j,Rn}$. These components together form a single test input x'_j . We plug these inputs into the hybrid mean prediction equation 12 and variance prediction equation 13 to compute the model's output distribution for a single output dimension. We repeat this to predict the output distributions for each pixel in the future image z_{i+5} which is stored as a mean and variance image tuple (M_{i+5}, V_{i+5}) .

Fourth Step and Onwards: The third step of the predictive rollout predicts z_{i+6} from input images $[z_{i+3}, z_{i+4}, z_{i+5}]$. For this and all subsequent predictions, all the input images are random variables outputted by our model. To predict the future image we utilize the approach detailed in the section 4.3 on Prediction with all random inputs.

A.4 Training Input Creation Graphic

The Figure 5 graphically demonstrates the process of creating a training datapoint from patches of 4 consecutive video frames.

A.5 Additional Experiments and Details

Predictive Comparison Experiment: Additional Details

In this section we highlight additional details on the methodology used to generate the results for the 'Predictive Comparison' Experiment in Section 5. To compare all three methods, we predict frames $[z_{10}, \dots, z_{24}]$ given frames $[z_0, \dots, z_9]$. For our method we train our model using $[z_0, \dots, z_9]$ and begin our prediction with input images $[z_7, z_8, z_9]$, identical to the approach outlined in the 'Forward Prediction' Experiment.

The FNO-2d-time model convolves across the two spatial dimensions to predict a single future image with a recurrent structure in time. This model uses a rollout method to predict longer video sequences. The model predicts one future frame at a time and incorporates its last prediction into its next input. We continue this until we have predicted the desired number of frames. The model is structured to take an input of three images and predict a single future image. We train this method in a manner similar to ours. The training data is created using the first 10 frames $[z_0, \dots, z_9]$. These frames are separated into data points of 4 consecutive images $[z_i, \dots, z_{i+3}]; \forall i \in [0, 6]$, where the first three images form the input and the fourth is the output. The model is trained over 20 epochs. The trained model is then used to predict 15 frames $[z_{10}, \dots, z_{24}]$ of the same sequence.

The FNO-3d model is a neural network that convolves in space and time to directly output several frames from a set of input frames. We train this model using the first 25 frames from two unique sequences, generated using the same simulation parameters. The first 10 images are used as the inputs, with the remaining 15 serving as the training outputs. Once trained over 20 epochs this model is given a set of 10 consecutive frames $[z_0, \dots, z_9]$ to predict the next 15: $[z_{10}, \dots, z_{24}]$.

The results of this comparison are shown in fig. 4.

Average Result Metrics

We showcase the average relative error and average mean standard deviations off of our model's predictions evaluated on 100 separate video sequences in Figure 7. For each video sequence our model is trained using the first 10 frames $[z_0, \dots, z_9]$ and used to predict the next 15 frames, $[z_{10}, \dots, z_{24}]$. We use the parameters discussed in the 'Forward Prediction' experiment.

Sequential Prediction Experiment:

In this experiment we examine the benefits of incorporating recent data into our model. We incrementally train models with the first 5, 10 and 15 images of a video sequences. Each of these models is used to predict 15 frames into the future, starting from their last training image. In Figure 6 we can visually see the improvement in prediction accuracy as we update our models. In the relative error graph (Figure 6c) we also show the results of starting predictive rollouts for the lower data models, trained with 5 and 10 images, later in the sequence. This provides a fair evaluation to compare the impact of adding recent data, by mitigating the added error compounded as a result of the predictive rollouts. The graph shows a large improvement in accuracy as we incorporate data into our model.

Additional Visual Results

Figures 8 and 9 show additional results for predictions on different Navier Stokes simulations using the "Forward Prediction Experiment" detailed in section 5.

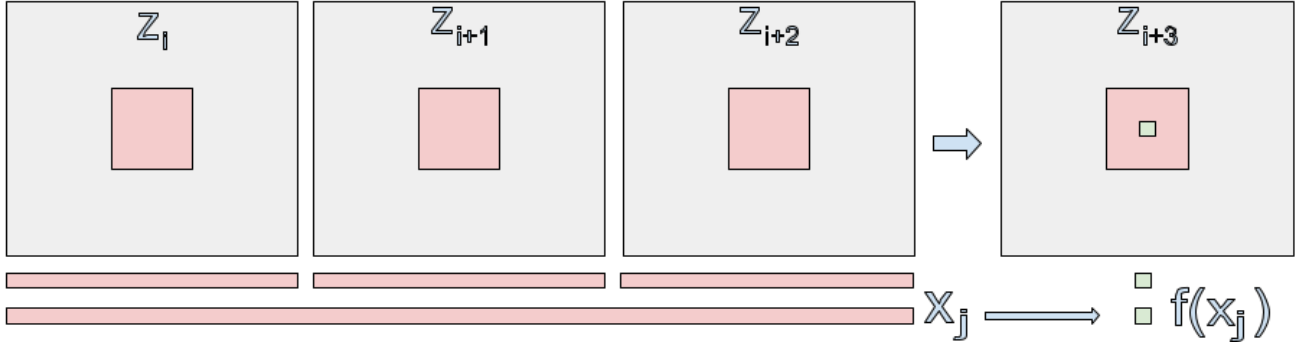


Figure 5: Graphic to visualize the process of generating a training data point from a sequence of 4 consecutive video frames. Each grey figure represents a labelled video frame. The red squares represent the patches that are sampled to create the input output pair. In the fourth image the green pixel represents the output patch after cropping the patch with patch border b . The patches from the first 3 images are flattened and concatenated to form the input. The patch from the fourth image is flattened and used as the output. In this case the output patch is a single pixel.

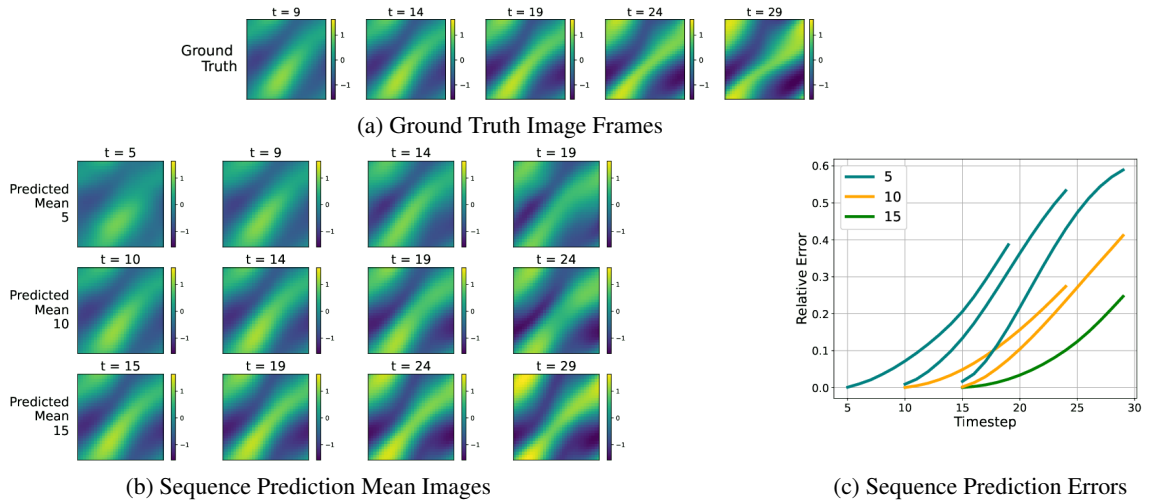
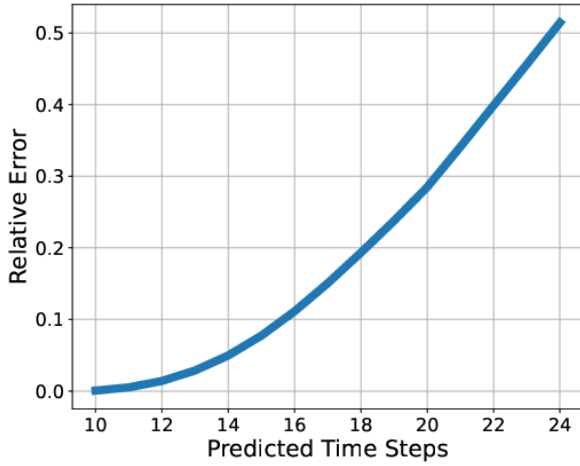
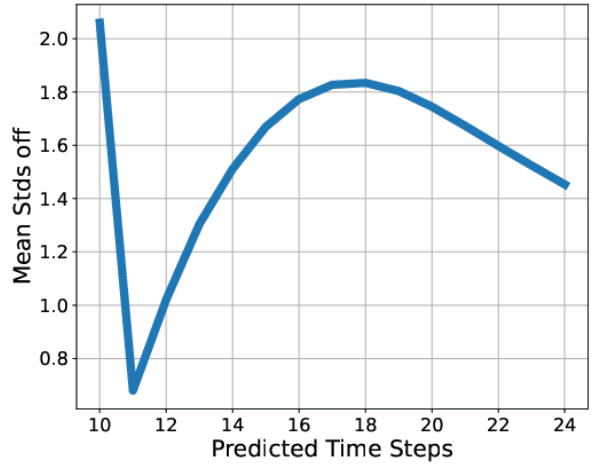


Figure 6: Sequential Prediction Experiment: Our model, trained using frames $[z_0, \dots, z_{t_0-1}]$, is used to predict frames $[z_{t_0}, \dots, z_{t_0+15}]$ of a 2D Navier Stokes simulation. Prediction results for $t = 5, 10, 15$ are shown along the rows of 6b, respectively. Figure 6a displays ground truth images. Figure 6b shows the predicted mean images. Figure 6c displays a graph of the relative error of the predicted means. In Figure 6c we show additional error results where we start predictive rollouts with the models trained with 5, 10 images from later time steps. This provides a fair experiment to show the predictive improvement resulting from incorporating recent data into our model.

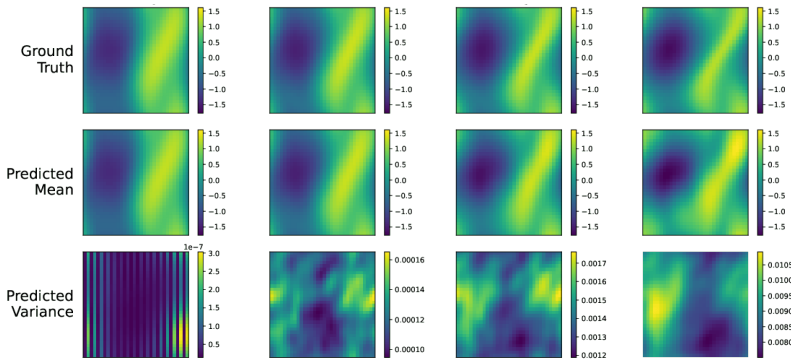


(a) Average Relative Errors

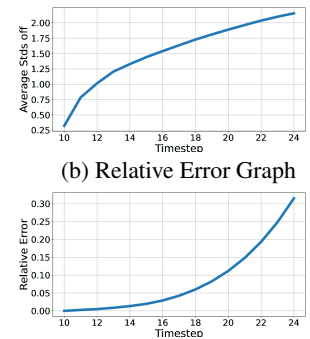


(b) Average Mean Standard Deviations off

Figure 7: Averaged Metrics: Figure 7a Shows the average relative error metrics using our method over 100 results on separate video sequences. Figure 7b Shows the average mean standard deviations off the predicted image is from the ground truth using the mean and variance generated using our method. This result is also averaged over predictions on 100 different video sequences. To generate the above results our model was trained on frames $[z_0, \dots, z_9]$ of each sequence and used to predict the next 15 frames, $[z_{10}, \dots, z_{24}]$

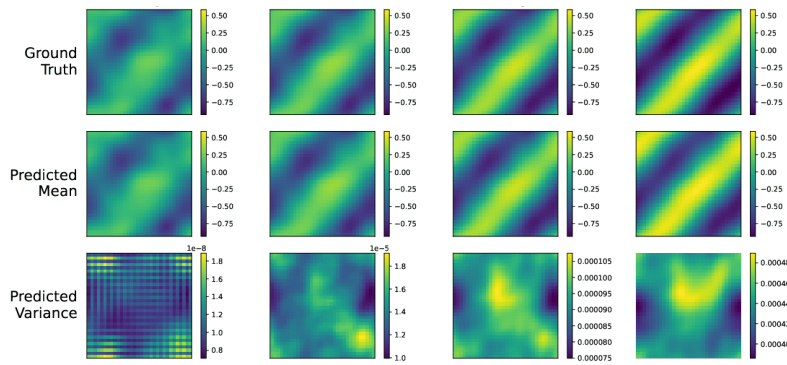


(a) Forward Prediction: Image Results

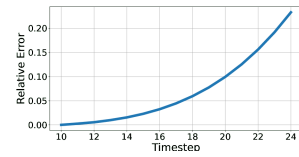


(c) Mean Standard Deviations off

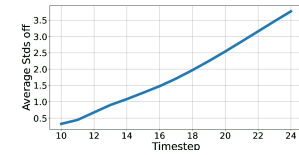
Figure 8: Forward Prediction Experiment: Additional Experiment 1: Our model, trained using frames $[z_0, \dots, z_9]$, is used to predict frames $[z_{10}, \dots, z_{24}]$ of a 2D Navier Stokes simulation. Figure 8a shows the ground truth, predicted mean and variance images. Figure 8b and Figure 8c show graphs of the prediction's relative error and mean standard deviations off.



(a) Forward Prediction: Image Results



(b) Relative Error Graph



(c) Mean Standard Deviations off

Figure 9: Forward Prediction Experiment: Additional Experiment 2: Our model, trained using frames $[z_0, \dots, z_9]$, is used to predict frames $[z_{10}, \dots, z_{24}]$ of a 2D Navier Stokes simulation. Figure 9a shows the ground truth, predicted mean and variance images. Figure 9b and Figure 9c show graphs of the prediction's relative error and mean standard deviations off.